

Article

Alleviation Effects of Hoods at the Entrances and Exits of High-Speed Railway Tunnels on the Micro-Pressure Wave

Weibin Ma ^{1,2}, Yufei Fang ^{1,2}, Tao Li ³ and Mingyu Shao ^{3,*} 

¹ State Key Laboratory for Track System of High-Speed Railway, Beijing 100081, China; dwangfei@163.com (W.M.); yffang@buaa.edu.cn (Y.F.)

² Railway Engineering Research Institute, China Academy of Railway Sciences Co., Ltd., Beijing 100081, China

³ School of Transportation and Vehicle Engineering, Shandong University of Technology, Zibo 255000, China; 20502030196@stumail.sdut.edu.cn

* Correspondence: shaomingyu@sdut.edu.cn

Abstract: The MPW that emits from a tunnel's exit when a high-speed train passes through is a serious environmental problem which increases rapidly with the speed of the train. To alleviate the MPW problem at 400 km/h, the aerodynamic effects caused by the hood located at the entrance or exit of a tunnel are studied by numerical method, and the influences of hood geometry, such as an enlarged cross-section, oblique entrance, and opening holes on the MPW, are also investigated. The research indicates that the enlarged cross-section of the hood at the entrance and exit of the tunnel has opposite effects on the MPW, and the oblique section can alleviate the MPW by extending the rising time of the compression wave and increasing the spatial angle at the hood exit. The pressure gradient can be mitigated through delaying the rising of the compression wave by opening holes on the side wall of the hood, and the relief effects of the holes can reduce the MPW further. The MPW problem when a train passes through a tunnel at 400 km/h can be effectively alleviated by an optimized oblique enlarged hood with opening holes, even up to train speeds of 500 km/h.

Keywords: micro-pressure wave; compression wave; high-speed train; noise and vibration



Citation: Ma, W.; Fang, Y.; Li, T.; Shao, M. Alleviation Effects of Hoods at the Entrances and Exits of High-Speed Railway Tunnels on the Micro-Pressure Wave. *Appl. Sci.* **2024**, *14*, 692. <https://doi.org/10.3390/app14020692>

Academic Editor: Tao Zhu

Received: 2 November 2023

Revised: 10 January 2024

Accepted: 11 January 2024

Published: 13 January 2024



Copyright: © 2024 by the authors. Licensee MDPI, Basel, Switzerland. This article is an open access article distributed under the terms and conditions of the Creative Commons Attribution (CC BY) license (<https://creativecommons.org/licenses/by/4.0/>).

1. Introduction

High-speed railways have become an important part of transportation, with advantages of safety, comfort, and convenience. When a train passes through environments such as mountains, rivers, and buildings, aerodynamic problems such as train wind, pressure wave, noise, and micro-pressure waves will be induced. The micro-pressure wave (MPW) is generated by the compression wave propagating outward from the tunnel exit, and is formed when a train enters the tunnel. Serious problems such as structural vibration and noise near the line will be caused by the MPW, and even a sonic boom can be induced, which may affect the health of residents surrounding the tunnel exit [1]. The micro pressure wave value at the exit of the tunnel is directly proportional to the pressure gradient inside the tunnel, and the pressure gradient value directly depends on the train speed [2]. With the development of high-speed rail technology, the running speed of trains gradually increases, and the problem of micro-pressure waves generated by trains entering the tunnel becomes more serious. Therefore, the MPW is a critical environmental problem that must be solved in the construction of high-speed railways. Its formation can be divided into three stages: compression wave generation, propagation and evolution, and micro-pressure formation. Extensive studies have been carried out on the mitigation of the MPW according to its formation process.

The air in the tunnel is compressed violently when a train enters a tunnel at high speed, resulting in a sudden change in pressure, and a compression wave is formed. The intensity of the MPW is related to the pressure gradient of the compression wave, and various hoods set at the tunnel entrance have been found to be effective in reducing the gradient of the

compression wave [3,4]. Bellenoue [5] studied the effects of the blind hood with a section on the generation of compression waves through reduced scale experiments; the results showed that a unique optimum hood exists for a fixed train/tunnel blockage ratio. Saito [6] conducted a model experiment to investigate the effective composition of an unvented hood, and the optimum cross-section area and length of the hood were obtained at 350 km/h. Fukuda [7] investigated the effect of the cross-section area of hoods using axisymmetric models; they found that a hood with multi-step cross-sections is more effective than those with a constant cross-section. Zhang [8–10] studied the effects of different tunnel portals on tunnel aerodynamics using a moving model test; the results indicated that the hat oblique portal combined with a buffer structure with top holes is particularly effective. Auvity [11] revealed that opening holes on the hood can delay the rising time of the compression wave further by splitting the wavefront into multiple stages. Anthoine [12] carried out a parametric investigation using a model experimental facility to study the effects of different portals, which indicated that the progressive entrance has a relieving impact on the gradient of the compression wave. Kim [13,14] proposed an entrance hood with air slits, which are designed to bio-mimic the “ram ventilation” technique, and a subsequent reduction in the MPW was observed in the reduced scale model test. Howe [15–19] proposed a compression wave analysis method based on potential flow theory, and the influence of a portal on the initial thickness of the compression wave was studied. Numerical simulation is also widely used in the study of the tunnel portal. Zhang [20] studied the aerodynamic effects of a train passing through tunnels without and with a hood by numerical method, and an enlarged hood with an arch lattice-shell was proposed. Mok [21] studied the formation of compressed wavefronts for different hoods based on the three-dimensional compressible Euler equation.

When compressed waves propagate in tunnels, they tend to steepen gradually, influenced by inertia. Vardy [22] presented a numerical model to analyze the propagation of a wavefront along tunnels. Evolution experiments of the compression wave was tested at Euerwang tunnel in Germany [23], and the wave steepening was measured. Miyachi [24] carried out field measurements in Shinkansen; the results showed that the compression wave with a waveform of pressure that has shallow valleys steepen more easily. Fukuda [25] investigated the influence of ballast on the pressure gradient of the compression wave in railway tunnels based on actual vehicle tests, indicating that it has a relieving effect on the steepness of the compressive wave front. Wang [26] studied the wavefront propagation using FVM methods, and the simulation demonstrated the presence of the most unfavorable tunnel length. Rivero [27] proposed a one-dimensional model to investigate the propagation process of compressed waves in the tunnel, then the wall friction and heat transfer effects were analyzed.

When the compression wave propagates to the end of the tunnel, a part is released outside in the form of a pulse wave, forming the MPW. Mayachi [28] performed a model experiment to investigate the impacts of the environment around the tunnel exit on the MPW, and a modification of a prediction model for MPW amplitude was made based on the experimental results. Liu [29] conducted a series of field measurements to study the MPW and the transient pressure, which obtained the variation of the MPW with the position and train's speed. The mitigation methods of the MPW can be divided into two types, active and passive. The passive means reduces the MPW using a hood with the inside partition at the tunnel exit portal [30], while the active methods of alleviation are intended to generate pressure disturbances equal and opposite to the MPW that would exist in their absence [31]. In engineering practice, several opening holes with small area can be set on the exit portal to reduce the MPW emitting from the tunnel.

The entrance hood is a main approach to mitigating the MPW by delaying the rising time of the pressure, which is effective when the train speed is less than 350 km/h. With the continuous progress of high-speed railways, train speeds increase continuously. The experimental speed has reached Mach 0.5 [32], and the maximum speed of a single train in the tunnel reaches 403 km/h. It is difficult to satisfy the MPW mitigation requirement

at the speed of 400 km/h or above solely using the entrance hood. The tunnel hoods in existing research mostly have top openings, which can cause difficulties in operation and maintenance under the influence of falling rocks and other factors, and can easily lead to safety issues. In addition, a double-track railway is usually used in current designs, so the entrance hood is located at the tunnel's exit when the train runs in reverse directions, the effects of which on the MPW are rarely reported.

In summary, scholars have conducted extensive research on hoods at the tunnel entrance. Establishing a tunnel hood at the tunnel entrance can effectively alleviate micro-pressure waves, but it is difficult for the current tunnel hoods to meet the demand for mitigation at higher speeds, and there are many parameters that affect the tunnel hood. The numerical method is used to study the effects of the hood located at the entrance or exit of a tunnel on the compression wave and the MPW. Then, the influences of the cross-section area, oblique slope, and opening number of the hood are analyzed, and the optimum configuration of the hood installed in both the entrance and exit of the tunnel is also studied. The purpose of this study is to reduce the micro-pressure wave generated by trains entering tunnels at higher speeds, and to provide reference for the construction of tunnel hoods at speeds of 400 km/h or above.

2. Numerical Calculation Method

2.1. Governing Equation

The research methods for the aerodynamic effect of train tunnels mainly include theoretical analysis, actual vehicle testing, model experiments, and numerical simulation. Considering the advantages of low cost and convenient simulation of different working conditions in numerical simulations, this paper adopts the method of numerical simulation to analyze the MPW characteristics generated by trains entering tunnels with different hoods. The numerical simulation of the aerodynamic effects of high-speed railway tunnels is based on the fluid equation governed by the laws of physical conservation, including the conservation of mass, momentum, and energy, which can be expressed as:

$$\frac{\partial \rho}{\partial t} + \nabla \cdot (\rho \mathbf{u}) = 0 \tag{1}$$

$$\frac{\partial (\rho \mathbf{u})}{\partial t} + \nabla \cdot (\rho \mathbf{u} \mathbf{u}) = -\nabla p + \nabla \cdot (\boldsymbol{\tau}) + \rho \mathbf{g} \tag{2}$$

$$\frac{\partial (\rho E)}{\partial t} + \nabla \cdot (\mathbf{u}(\rho E + p)) = \nabla \cdot [k_{\text{eff}} \nabla T + (\boldsymbol{\tau} \cdot \mathbf{u})] \tag{3}$$

where t is time; ρ represents fluid density; \mathbf{u} denotes fluid velocity vector; p represents fluid pressure; \mathbf{g} denotes the gravity; $\boldsymbol{\tau}$ is the viscous stress tensor; E represents the sum of kinetic energy and internal energy; and k_{eff} represents the effective thermal conductivity coefficient. For Newtonian fluid, the viscous stress is proportional to the deformation rate of the fluid, which can be described as:

$$\boldsymbol{\tau} = \mu \left[(\nabla \mathbf{u} + \nabla \mathbf{u}^T) - \frac{2}{3} \nabla \cdot \mathbf{u} \mathbf{I} \right] = \mu \left[\left(\frac{\partial u_i}{\partial x_j} + \frac{\partial u_j}{\partial x_i} \right) - \frac{2}{3} \frac{\partial u_k}{\partial x_k} \sigma_{ij} \right] \tag{4}$$

where μ is the dynamic viscosity of air, and \mathbf{I} represents unit tensor.

Air based on the *ideal gas* model is adopted in this study, and the density for compressible flows can be obtained by $\rho = (p_0 + p)/RT$, where p_0 is the operating pressure, and R denotes the specific gas constant. For air at near-standard conditions, $R = 287 \text{ J}/(\text{kg}\cdot\text{K})$. The dynamic viscosity is derived by *Sutherland's law* with three coefficients, which can be expressed as:

$$\mu = \mu_0 \left(\frac{T}{T_0} \right)^{3/2} \frac{T_0 + S}{T + S} \tag{5}$$

where μ_0 and T_0 denote the reference viscosity and reference temperature, respectively; and S is the Sutherland constant. For air at moderate temperature and pressure, $\mu_0 = 1.716 \times 10^{-5}$ kg/(m·s), $T_0 = 273$ K, and $S = 111$ K. The effective thermal conductivity coefficient is calculated according to the turbulence model, and the RNG k - ϵ turbulence model is used [33]. The model constants are given as $C_\mu = 0.0845$, $C_{1\epsilon} = 1.42$, and $C_{2\epsilon} = 1.68$, and the turbulent Prandtl number at the wall is fixed as $Pr_t = 0.85$. Since the source terms and species diffusion are not involved in this study, the values of S_m , S_h , and J_j are zero.

Although the variables of the three governing equations are different, they all represent the conservation of the physical quantities in the fluid. If the general variable in the equation is represented by ϕ , the governing equation can be written in the following general form:

$$\frac{\partial(\rho\phi)}{\partial t} + \nabla \cdot (\rho\mathbf{u}\phi) = \nabla \cdot (\Gamma\nabla\phi) + S_\phi \quad (6)$$

The left two terms represent the transient and convective terms, respectively, while the right two terms represent the diffusion and source terms, respectively. For a specific equation, ϕ , Γ , and S_ϕ have a specific form. Through appropriate mathematical processing, the variables, transient terms, and diffusion terms can be organized into the standard form of the above equations, and the remaining terms can be defined as source terms, thereby transforming to a universal form of the governing equation.

2.2. Geometry Model

The geometric shapes of trains and tunnels are very complex. In order to form a reasonable numerical model of tunnel aerodynamics, it is necessary to simplify the geometry of the train and tunnel. The high-speed train CR400AF is used, which consists of eight carriages with a total length of 211.3 m. The train is simplified into a smooth geometric body by ignoring structures such as pantographs, door handles, and bogies, as shown in Figure 1a. According to design specifications, when the train speed exceeds 350 km/h, the cross-section area of the double-track tunnel should not be less than 100 m². Considering the most severe conditions, the cross-section area is taken as $A_t = 100$ m², the distance between two lines as 5 m, and the tunnel length as $l_t = 647$ m. The influences of the track and ballast are also ignored, and the plane where the track is located is taken as ground. A maintenance passage with a width of 1.6 m and height of 0.3 m is also modelled, which is shown in Figure 1b. The oblique enlarged hood with opening holes is installed at the entrance and/or exit of the tunnel. The length and cross-section of the tunnel hood are denoted as l_h and A_h , respectively, and the oblique rate is defined as $k = d/h$. To avoid safety issues caused by factors such as falling rocks, two rows of holes are symmetrically arranged on both side of the hood, with a width of 3 m and height of 3.5 m. The number of the holes is denoted as n , and the spacing between two adjacent holes is 2 m, as shown in Figure 1c.

2.3. Computational Domain and Boundary Conditions

The computational domain of the tunnel aerodynamics consists of regions outside and inside of the tunnel. The size of the outside region is determined by the fact that the disturbance at the boundary should not have a significant impact on the MPW emitted from the tunnel. The numerical results show that the boundary of the outside region has almost no effect on the MPW when the diameter of which exceeds 300 m. Therefore, the diameter of the outside region is taken as $D = 300$ m. Both the boundary disturbance and the smooth acceleration of the train should be taken into consideration for the length of the outside region, and a length of $L = 550$ m is taken.

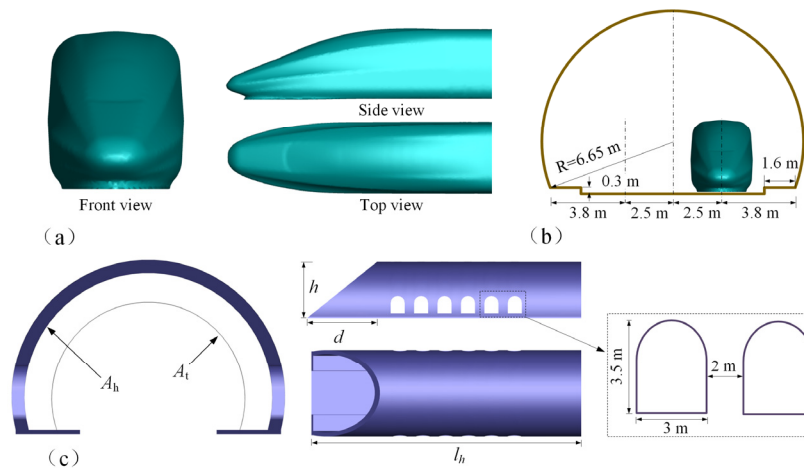


Figure 1. Schematic diagram of the geometric model: (a) Three views of the train nose; (b) Tunnel section; (c) Sketch of the hood.

The sliding mesh and dynamic layering are used to simulate the driving process of trains in tunnels. The entire computational domain consists of four parts, the moving domain around the train, deforming domains before and after the train, and the residual fixed domain, as shown in Figure 2. The moving domain includes trains moving forward at the same speed, while the deforming domain deforms as the train moves to maintain the boundary of the stationary computational domain. The *Interface* boundary condition is used for data exchange between two adjacent domains.

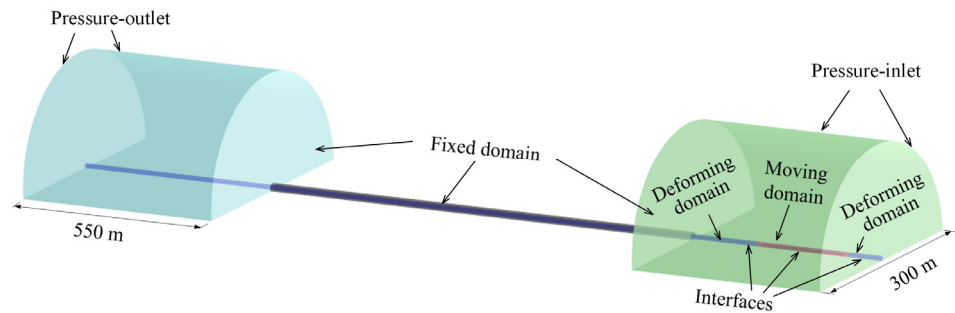


Figure 2. Computational domain and boundary conditions.

When the speed of the train increases directly from zero to the specified running speed, abnormal compression waves will be generated. To eliminate the effects of the sudden start on the compression wave, a polynomial velocity curve is used when the train accelerates [34]:

$$v(t) = \frac{a}{20}t^5 - \frac{at_a}{8}t^4 + \frac{at_a^2}{12}t^3 \tag{7}$$

where $a = 120 v_t/t_a^5$, t_a denotes the acceleration time of the train, and v_t represents the train speed. When the train moves forward, for any control volume in the moving domain, the governing equation in integral form can be expressed as:

$$\frac{d}{dt} \int_{CV} \rho \phi dV + \int_{CS} \rho (\mathbf{u} - \mathbf{u}_g) \cdot \mathbf{n} dA = \int_{CS} \Gamma \nabla \phi \cdot \mathbf{n} dA + \int_{CV} S_\phi dV \tag{8}$$

where CS is boundary of the control volume CV , \mathbf{u}_g is the velocity vector of the dynamic mesh, and \mathbf{n} is the normal vector of the surface element dA .

Pressure-Inlet is applied to the boundary of the region outside the tunnel entrance, while that of the region outside the tunnel exit is set as *Pressure-Outlet*. The *Non-Reflecting* condition in the *Acoustic Wave Model* is activated to eliminate disturbances from the boundary reflection.

2.4. Monitoring Points

To study the influences of the hood on the compression wave, two monitoring points are arranged symmetrically on the tunnel 200 m away from the entrance, which are marked as LP and RP, respectively. In numerical simulation, the variation of pressure and its gradient of these points are monitored. Another two monitoring points are located in the exit hood 20 m away from the tunnel exit, marked as LH and RH, which are parallel to LP and RP, respectively. In addition, two monitoring points denoted as LM and RM are set at 20 m outside the tunnel or hood, as shown in Figure 3.

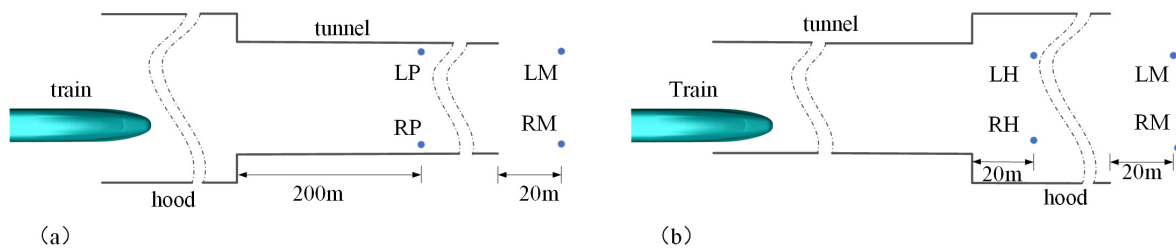


Figure 3. Monitoring points in the simulation: (a) Hood at tunnel entrance; (b) hood at tunnel exit.

2.5. Grid Scheme

Hybrid grids are adopted to satisfy both accuracy and efficiency of the numerical simulation. For the moving domain, unstructured grids are used due to the complex shape of the train. The deformation domains before and after the train, which have regular shapes, can be meshed by high-quality structured grids as shown in Figure 4a. The adjacent domains are connected by setting node coincidence on the overlap boundaries. Although there are hood structures and other structures in the fixed domain, the structured grids are still feasible to the fixed domain, as shown in Figure 4b.

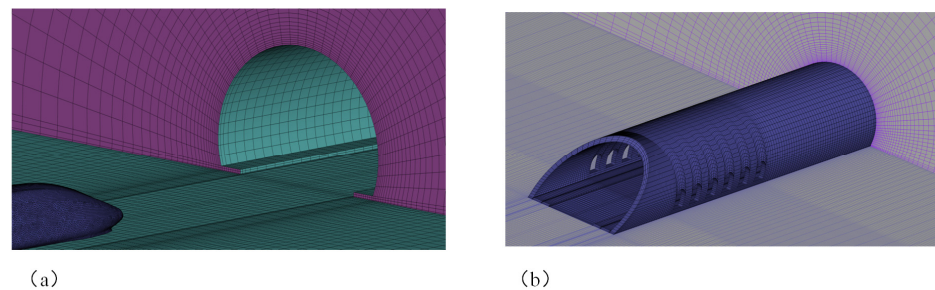


Figure 4. Grid distribution of the model: (a) Mesh of tunnel and train; (b) Mesh of hood.

3. Numerical Method and Validation

The numerical method used in this paper is validated with the results of field measurement [35]. A train with 8 carriages was used in the test, which had a total length of 201.4 m and a cross-section area of 11.2 m², passing through the tunnel at 300 km/h. The tunnel had the same cross-section as that mentioned in this paper, and a total length of 1005 m with ballast-less tracks laid inside. The atmospheric pressure of the test ground was 1.02×10^5 Pa, and the ambient temperature was 8.9 °C. During the testing, measurement points were arranged at 140 m from the entrance with a height of 1.5 m to monitor the pressure variation.

The convergence of the mesh is studied first. The grid sizes may affect calculation accuracy; therefore, four sets of mesh with different quantities (denoted as N) are modelled by changing the sizes of grids. *ANSYS Fluent* is used to solve the fluid governing equation. The coupling between velocity and pressure is dealt with using the *Semi-Implicit Method for Pressure Linked Equations*, and the gradient term is discretized by the *Green-Gaussian Cell-Based* method. The pressure term is discretized using the *standard* format, and the *second-order upwind* format is adopted in the discretization of the other spatial terms. In addition, the *second-order implicit* format is used in the time discretization.

The peak–peak pressure differential of the measurement point inside the tunnel and the amplitude of the MPW 20 m outside the tunnel exit with different meshes are shown in Table 1. The results show that when $N > 7.990 \times 10^6$, the variation in Δp and $(\Delta p_m)_{\max}$ can be ignored. Therefore, the grid sizes used in *Mesh 3* are taken in the subsequent calculation. The minimum size of the grids on the train surface is 60 mm, which is set to 100 mm to the surfaces of the tunnel and hood. Boundary layers with a total number of 5 and a height of 1 mm for the first layer are arranged near the surfaces of train, tunnel, and hood.

Table 1. The pressure differential and amplitude of the MPW with different meshes.

Parameters	Mesh 1	Mesh 2	Mesh 3	Mesh 4
Grid quantity	6.329×10^6	7.354×10^6	7.990×10^6	8.945×10^6
Δp (kPa)	2.785	2.591	2.597	2.598
$(\Delta p_m)_{\max}$ (Pa)	60.17	59.44	59.39	59.26

Using the mentioned numerical model, the calculated pressure of the monitoring points 140 m and 400 m away from the tunnel entrance are compared with the filed measurement results, as shown in Figure 5. The pressure variation obtained by numerical simulation is basically consistent with that from field measurements. The relative errors of the peak–peak pressure differential compared to the experimental data are 0.74% and 2.86%, respectively. The numerical calculation results are in good agreement with the filed measurement data, indicating that the numerical method used in this paper can accurately simulate the aerodynamic effects caused by a train passing through a tunnel.

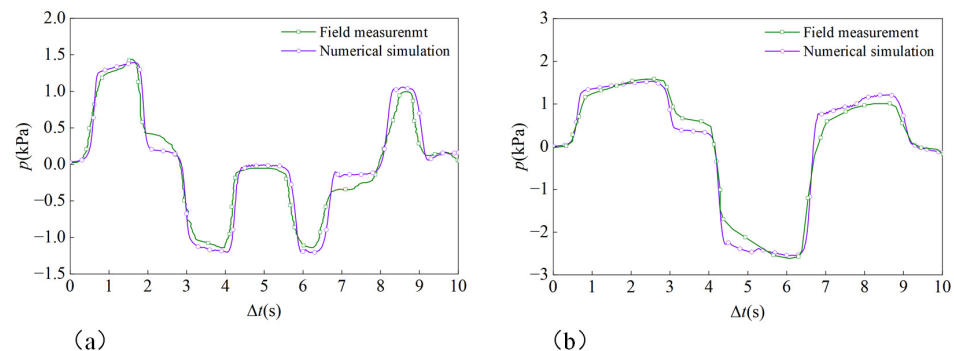


Figure 5. Comparison of pressure obtained by numerical simulation and field measurement: (a) Pressure at 140 m; (b) Pressure at 400 m.

4. Results and Discussion

The hood may be located at the entrance or exit of a tunnel depending on the direction the train enters. Therefore, different types of entrance hoods and exit hoods are studied to obtain the effects of the hood geometry on the compression wave and the MPW, and the optimum hood installed at both the entrance and exit of the tunnel is also analyzed. The standard condition of air is selected as the unperturbed condition, with $p_0 = 101,325$ Pa and $T = 288.15$ K in the subsequent study.

4.1. Hoods at Tunnel Entrance

The mitigation mechanism for the MPW due to enlarged hoods, oblique hoods, and hoods with opening side holes are studied first. As is well known, the compression wave has three-dimensional characteristics only at the initial stage of formation, transforming into a one-dimensional plane wave after going a certain distance in the tunnel. So, only the pressure characteristics of the right monitoring point are analyzed in subsequent studies. The reference values for the geometric parameters of the hood in the calculation are as follows: $A_h = 155$ m², $k = 1.25$, $n = 4$. When a train passes through the tunnel with different types of hoods (shown in Figure 6a) entering at a speed of 400 km/h, the pressure characteristics of the RP point and the MPW at the RM point are shown in Figure 6b,c.

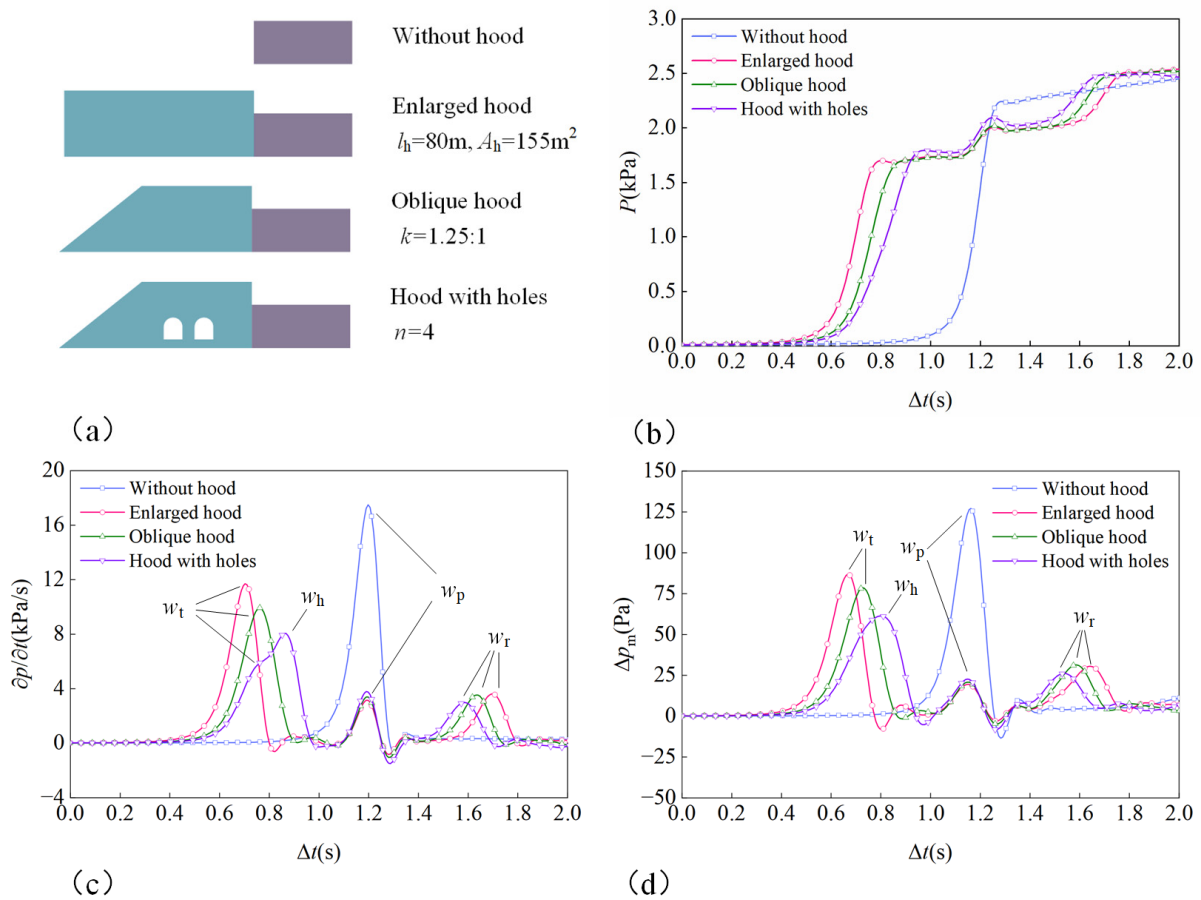


Figure 6. Comparison of tunnel aerodynamics with different types of hoods: (a) Tunnel with different hoods; (b) Pressures at RP point; (c) Pressure gradient at RP point; (d) MPW at RM point.

When an enlarged hood is installed at the entrance of the tunnel, the rising process of the compression wave is divided into three stages, corresponding to three small waves. When the train enters the hood, the surrounding air is compressed to generate the first wave (w_t), and the air in front of the train is compressed further as the train enters the tunnel, resulting in a second compression wave (w_p) and an expansion wave propagating to the rear. The expansion wave is reflected into a new compression wave (w_r) at the hood entrance, causing the third increase in pressure. The compressibility effects caused by the train entering the hood can be attenuated by an oblique entrance, leading to a decrease in the pressure gradient of w_t . The time when the pressure gradient peak appears is also delayed. When several opening holes are arranged at the side wall of the hood, a relief effect is induced to the pressure gradient of w_t , while a new compression wave w_h is generated as the train passes through the openings, which tends to overlap with w_t . Subsequently, when the train enters the tunnel, w_p appears at the same time as other hoods, but the intensity increases slightly. The time when w_r arrives is earlier, with a decrease in the intensity due to the opening holes. The MPW at the measuring point 20 m outside the tunnel (RM point) is shown in Figure 6d. The variation of the MPW is basically the same as that of the pressure gradient, except for that the waves w_t and w_h superimpose into one wave (denoted as w_h) when the hood with holes is adopted.

The maximum values of the pressure gradient of the compression wave and the MPW with the mentioned four hoods are shown in Table 2. The values of $(\partial p / \partial t)_{\max}$ and $(\Delta p_m)_{\max}$ decrease by 53.97% and 51.80%, respectively, compared to that without a hood, which means that the rising process of the compression wave can be extended effectively by an oblique enlarged hood with opening holes, resulting in the mitigation of the MPW.

Table 2. Maximum values of the pressure gradient and MPW with different hoods.

Type of Hoods	$\partial p/\partial t$		Δp_m	
	Maximum Value (kPa/s)	Mitigation Rate	Maximum Value (Pa)	Mitigation Rate
Without hood	17.49	/	130.20	/
Enlarged hood	11.70	33.10%	88.90	31.72%
Oblique hood	9.93	43.22%	80.40	38.25%
Hood with holes	8.05	53.97%	62.76	51.80%

The aerodynamics of hoods with different lengths ($l_h = 30\text{--}80\text{ m}$) are simulated to investigate the effects on the compression wave and the MPW. The pressure gradient at the RP point and the MPW at the RM point are shown in Figure 7.

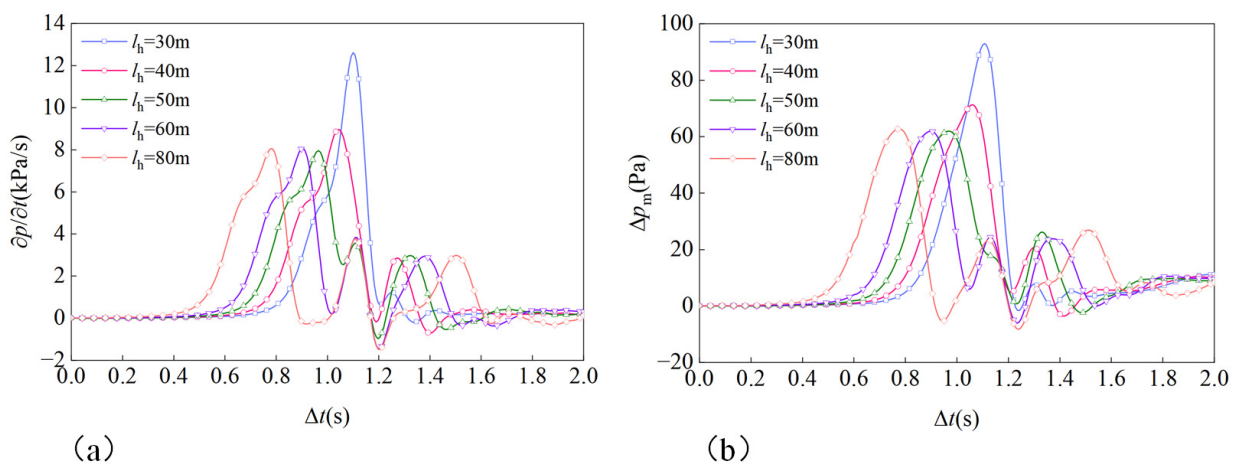


Figure 7. The effects of hood length on tunnel aerodynamics: (a) Pressure gradient at RP point; (b) MPW at RM point.

For all lengths, there are two peaks marked as w_t and w_h in the first stage of compression wave, which superpose together before they propagate to the tunnel exit. As the length of the hood increases, the time when w_t and w_h appear earlier with w_r delays gradually, while the time when w_p arrives remains unchanged. When the hood length is less than 40 m, w_h tends to overlap with w_t during the propagation, even with an inclination of superposing with w_r , leading to a significant increase in the pressure gradient and the MPW. When $l_h < 50\text{ m}$, the amplitudes of the pressure gradient and the MPW do not change with the length of the hood. Therefore, a sufficient length should be ensured, but excessive length cannot provide further relief effects. In subsequent calculations, $l_h = 80\text{ m}$ is taken to eliminate the influences of hood length on the tunnel aerodynamics.

The pressure gradients of the compression wave at RP point with different cross-section areas of hood are shown in Figure 8a. When $A_t > 200\text{ m}^2$, the pressure gradient of w_p is greater than w_h , which indicates that the compressibility effect caused by a train entering a tunnel plays a dominant role. With the decrease of the cross-section area, the compressibility effect of the train entering the tunnel weakens, resulting in the decrease of the pressure gradients of w_h and w_r . However, the compressibility effects of the train entering the hood and passing through the opening increase, leading to the increase and distinction of the pressure gradients of w_t and w_h , which means w_h is dominant.

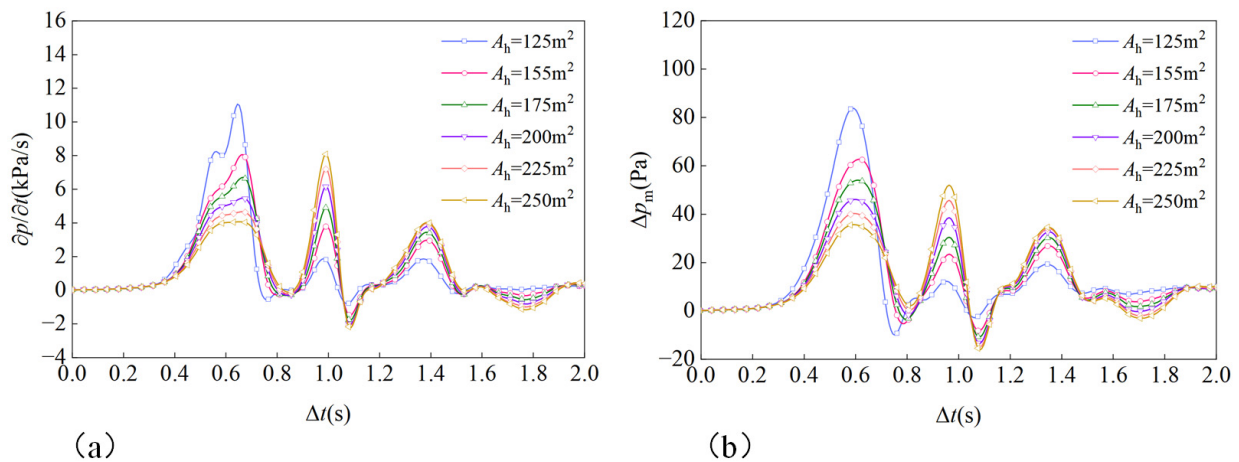


Figure 8. The effects of cross-section area of entrance hood on tunnel aerodynamics: (a) Pressure gradient at RP point; (b) MPW at RM point.

The MPW at RM point with varied hood cross-section areas is shown in Figure 8b. The waves w_t and w_h have been superimposed into a single wave (denoted as w_h) due to the influence of inertial effects, and the superposition effect is more significant with a smaller hood area. Affected by this, the MPW caused by the train entering the tunnel will surpass other effects when a larger hood area is adopted.

Therefore, there is an optimal hood area where the compressibility effects of the train passing through the holes and entering the tunnel are equivalent, thereby minimizing the amplitude of the MPW. Figure 9 shows the variation of the peak values of the pressure gradient and the MPW of the three stages. The curves show that the first peak decreases with increasing area, while the second and third peaks increase. The minimum value of the pressure gradient appears near $A_t = 200 \text{ m}^2$, while the minimum value of the MPW appears near $A_t = 225 \text{ m}^2$, which means that the optimal hood area is related to the tunnel length due to the inertia effect. In addition, when $A_t > 155 \text{ m}^2$, the change rate of the first peak decreases gradually. Considering factors such as construction costs, $A_t = 155 \text{ m}^2$ is used in subsequent calculations.

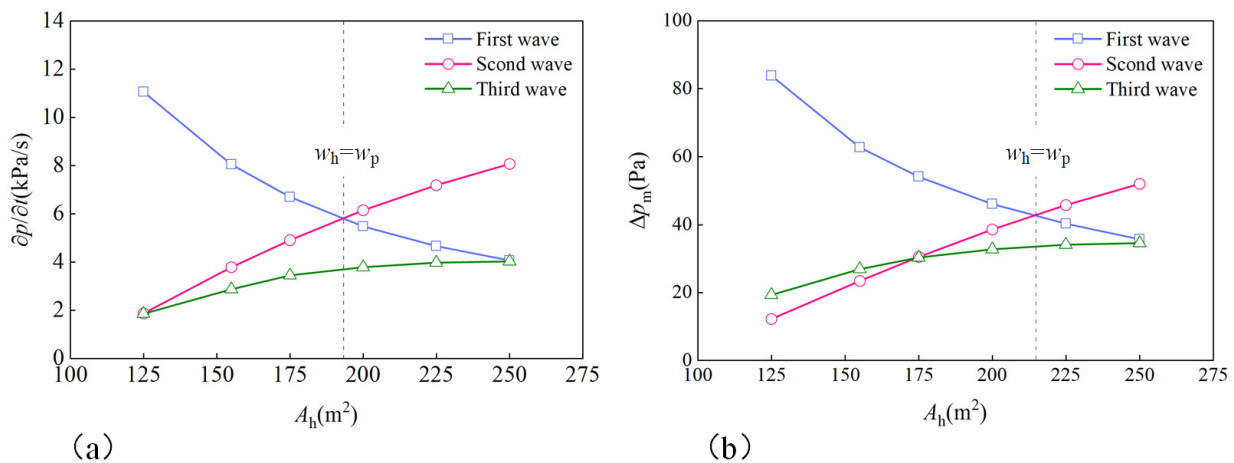


Figure 9. The peak values of pressure gradient and MPW of the three stages with different hood areas: (a) Pressure gradient at RP point; (b) MPW at RM point.

The pressure gradient caused by the train entering the hood can be weakened by an oblique entrance. The pressure gradient at the RP point when different oblique rates of the hood entrance adopted is shown in Figure 10a. The effective area and the length of the hood entrance increase with the oblique rate, resulting in a decrease of w_t —which is caused by the compressibility effect when a train enters the hood—while the intensity of w_h increases gradually. The pressure gradient of w_t is about the same as that of w_h when $k = 0.5$, which corresponds to the minimum pressure gradient. At the same time, the waveform of the MPW is changed due to the superposition effect during the propagation of the compression wave, leading to a decrease in the MPW with the increasing oblique rate, as shown in Figure 10b.

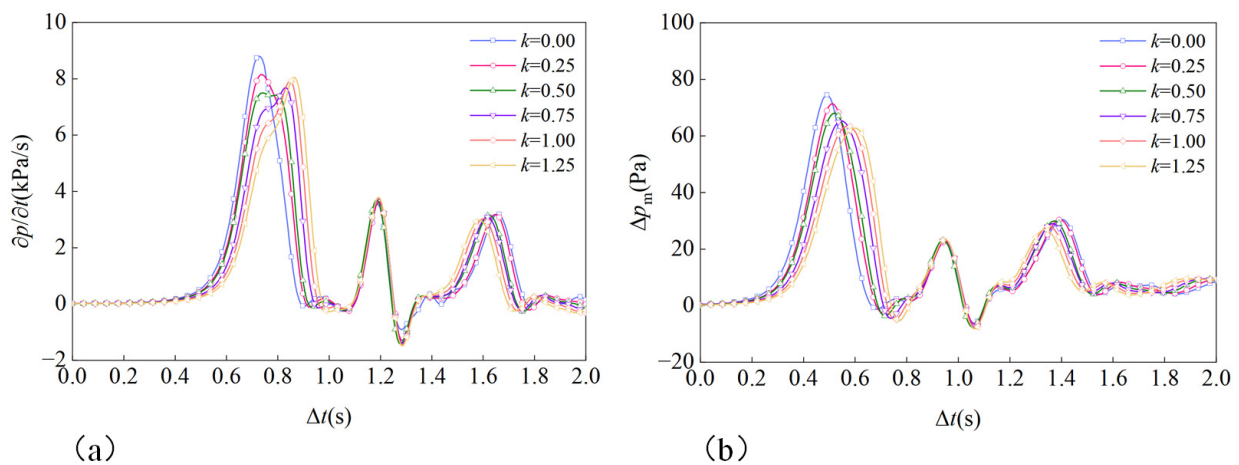


Figure 10. The effects of oblique hood entrance on tunnel aerodynamics: (a) Pressure gradient at RP point; (b) MPW at RM point.

In addition, when the slope of the entrance hood changes, the micro pressure wave (w_p) caused by the train entering the tunnel and the micro pressure wave (w_r) caused by the reflected compression wave basically do not change with the slope. The micro pressure wave (w_h) caused by the complete entry of the train into the tunnel hood dominates, and its peak value decreases with the increase of the slope, which can be approximated as:

$$(\Delta p_m)_{\max} = 12.796e^{-k/0.494} + 61.737 \tag{9}$$

Actually, the intensity of the MPW remains basically unchanged when $k > 1$, so $k = 1.25$ is taken.

The influences of the number of holes on the formation and evolution of the compression waves are also studied. When the number of holes ranges from 0 to 24, the pressure gradients of the RP point is shown in Figure 11a. The wave w_h appears obviously in the waveform and begins to play a dominant role when $n > 4$. Due to the influence of w_t , the wave w_h increases with the increasing number of holes. As the end of the opening moves away from the hood entrance ($n > 8$), the wave w_h decreases as the number of holes increases due to the weakened influence of w_t . At the same time, the wave w_h increases with the increasing holes number again due to the influence of w_p , as the end of the opening is closed to the tunnel entrance ($n > 12$). When the number of holes exceeds 20, w_h and w_p are superimposed into a single wave, leading to a rapid increase of the pressure gradient. The MPW exhibits the same variation compared with the pressure gradients as shown in Figure 11b; however, the superposition between w_h and w_t is more obvious due to the influence of the inertia effect. The distinction between w_h and w_t is inconspicuous when $n > 8$, while w_h and w_p are completely superimposed together for cases where $n > 18$.

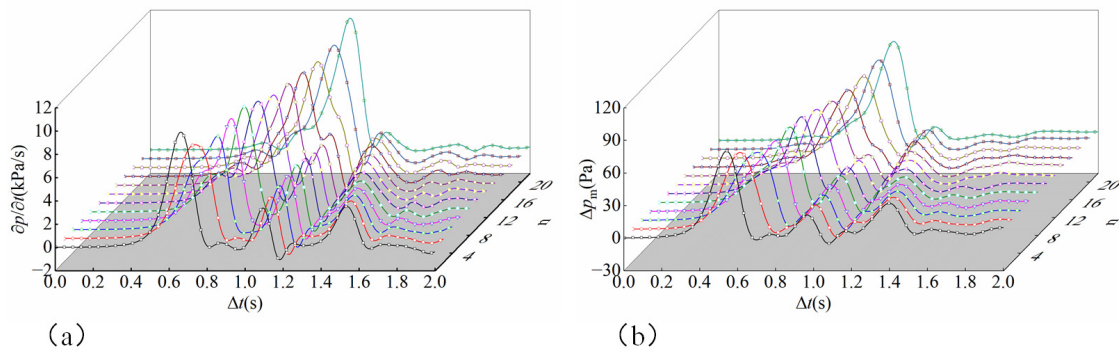


Figure 11. The effects of number of holes at entrance hood on tunnel aerodynamics: (a) Pressure gradient at RP point; (b) MPW at RM point.

Actually, the intensity of w_t is acceptable when $n = 6$, while the amplitude of w_h increases significantly due to its influence. The superposition effect of w_t and w_h can be weakened by moving the holes at the third row forwards (towards tunnel entrance). Figure 12 shows the pressure gradient and the MPW when the position of the holes at the third row changes, where i represents the position of the holes located at the third row originally. As the holes move forward, w_h is divided into two small waves, denoted as w_{h1} and w_{h2} . The pressure gradient amplitude of w_{h1} is about the same as that of w_{h2} when $i = 5$, which has the best alleviation effect on the MPW. In such a case, the amplitude of the MPW at RM point is $(\Delta p_m)_{\max} = 49.1$ Pa, which satisfies specification ($(\Delta p_m)_{\max} < 50$ Pa). In addition, the results show that the amplitude of the MPW can be reduced to 36.4 Pa by expanding the area to $A_t = 200$ m² while keeping other parameters unchanged, which is a decrease of 72.02% compared to that without a hood.

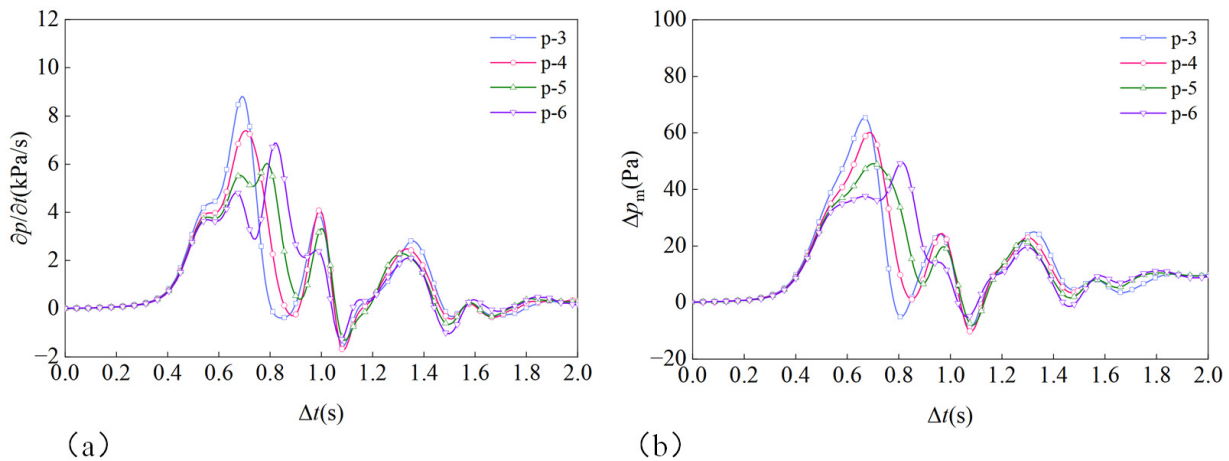


Figure 12. The effects of position of holes on tunnel aerodynamics: (a) Pressure gradient at RP point; (b) MPW at RM point.

4.2. Hoods at Tunnel Exit

The entrance hood will be located at the exit of the tunnel when the train runs in the reverse direction, the effects of which on the MPW is rarely reported. Therefore, the effects of the enlarged cross-section, oblique entrance, and holes on the side wall of the hood on the MPW are studied gradually based on the enlarged hood with a constant cross-section.

As the blind hood at the tunnel exit has little effect on the aerodynamics inside the tunnel, the waveform of the compression wave and the MPW will not change with the cross-section area. The maximum values of the pressure gradient at RH point and the MPW at RM point when a hood installed at the tunnel exit with different areas and a constant length of 80 m is show in Figure 13.

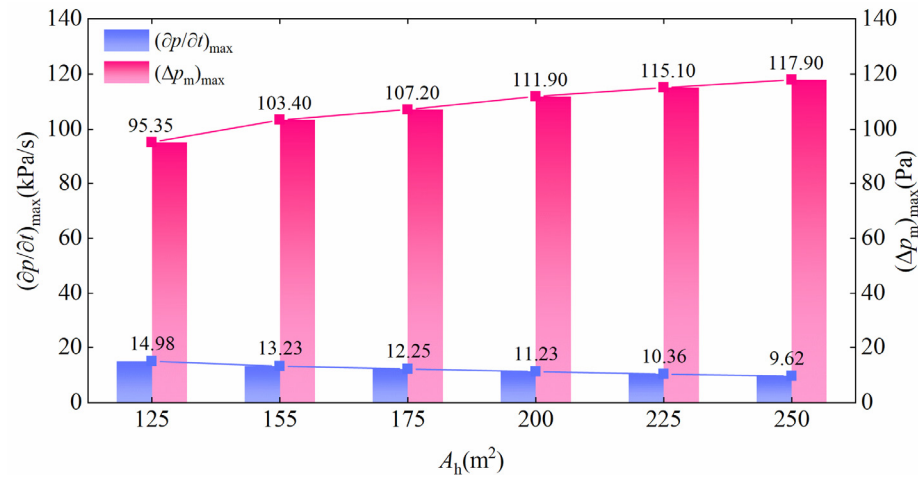


Figure 13. The effects of cross-section area of exit hood on the maximum values of pressure gradient and MPW.

As is well known, when the compression wave arrives at the exit of the tunnel, part of the energy enters the hood and propagates forward, while the other part propagates backwards as a reflected expansion wave. The results show that the intensity of the reflected expansion wave increases gradually with the hood area, while the compression wave propagating forward decreases, resulting in a mitigation of the pressure gradient at the RH point.

The MPW is generated from the energy radiating out from the compression wave, which propagates to the exit of the hood. According to the low frequency approximation theory, the amplitude of the MPW outside the exit can be expressed as:

$$\Delta p_m(r, t) = \frac{2A}{\Omega cr} \left(\frac{\partial p}{\partial t} \right) \tag{10}$$

where Ω is the spatial angle at the hood exit, $\partial p/\partial t$ represents the pressure gradient inside the hood, and r denotes the distance from the hood exit to the monitoring point. It is shown that that the amplitude of the MPW is proportional to the cross-section area of the hood and the pressure gradient at the hood exit, which increases as the area of the cross-section reduces. At the same time, the influence of the cross-section is dominant, resulting in an increase of the MPW intensity with the enlargement of the cross-section, which has an effect in contrast to the entrance hood. It is worth noting that the intensity of the MPW with a constant hood reduces compared to that without a hood due to a larger spatial angle. In addition, the change rate of the MPW slows down with the increasing area of the hood when $A_t > 155 \text{ m}^2$. Considering the requirement of the entrance hood, $A_t = 155 \text{ m}^2$ is taken in subsequent study.

The pressure contour of the hood with an oblique exit ($k = 1.25$) when the compression wave arrives is shown in Figure 14. The compression wave radiates out from the hood earlier with an enlarged radiating area, which means that the spatial angle can be increased by an oblique exit, resulting in a decrease in the amplitude of the MPW.

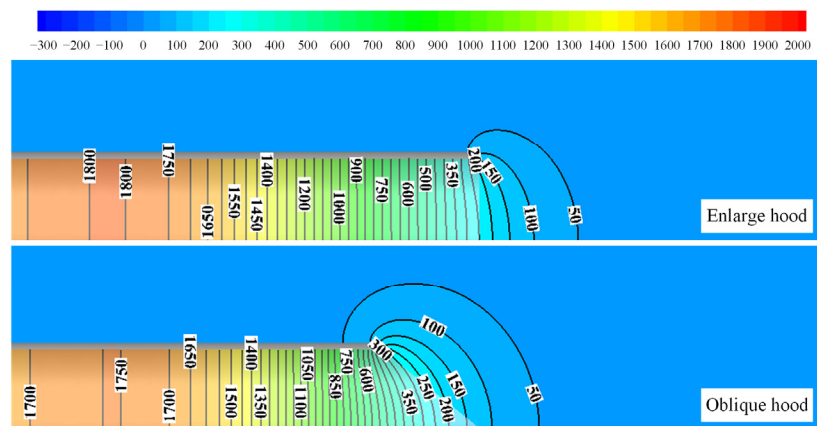


Figure 14. Pressure contours with different hood exits.

The amplitude of the MPW at the RM point with different oblique rate of the hood exit is shown in Figure 15. As the oblique rate increases, the intensity of the MPW decreases gradually due to the increasing spatial angle. The amplitude of the MPW can be reduced to 68.36 Pa when $k = 1.25$, which drops by 47.46% compared to that without any hood. Therefore, $k = 1.25$ is taken in subsequent calculation to be consistent with the hood at the tunnel entrance.

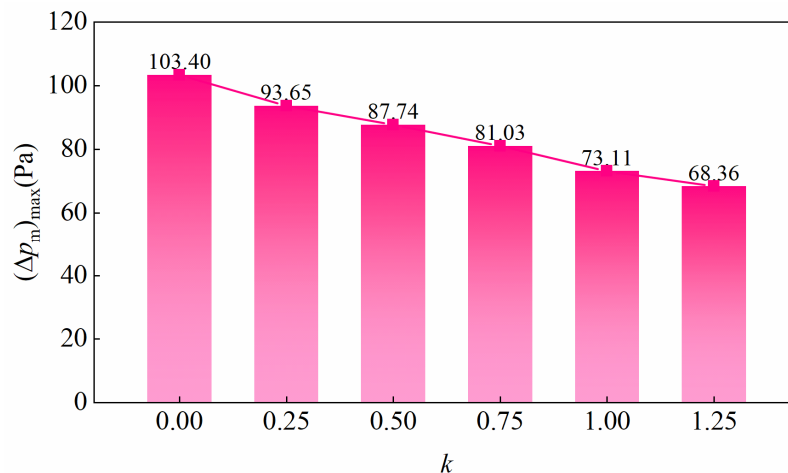


Figure 15. The effects of oblique hood exit on the MPW.

The pressure gradient of the compression wave in the exit hood can be further reduced by opening holes on the side wall, leading to a decrease in the MPW emitting from the hood. In addition, a reflected expansion wave is emitted backward when the front of the compression wave passes through the opening holes, which can further relieve the pressure gradient of the compressed wave. The variation of the gradient pressure at RH point with different number of holes on the hood is shown in Figure 16a.

With the increase in the number of holes, the opening area enlarges and approaches the monitoring point gradually, which leads to a stronger reflected expansion wave arriving earlier; then, the pressure gradient at RH point decreases correspondingly. The MPW at RM point with a varied number of holes on the hood is shown in Figure 16b. It is found that the amplitude of the MPW decreases rapidly with the increasing hole number due to the reflected expansion wave and the relief effect of the holes. The amplitude of the MPW can be reduced to 27.02 Pa when 22 holes is arranged on the hood symmetrically, which is 79.23% less than that without hood.

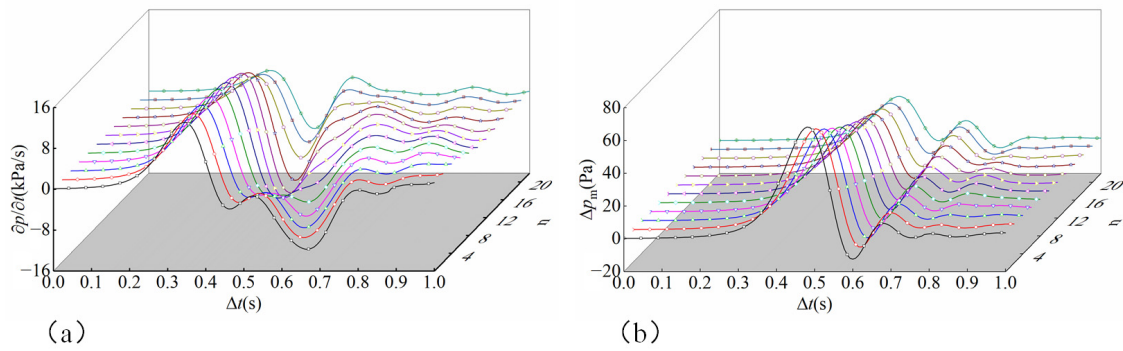


Figure 16. The effects of number of holes at the exit hood on tunnel aerodynamics: (a) Pressure gradient at RH point; (b) MPW at RM point.

4.3. Hoods at Both the Entrance and Exit of the Tunnel

The mentioned study shows that an oblique enlarged hood with opening holes installed at the entrance or exit can alleviate the MPW emitted from the tunnel. However, the geometric parameters of the hood located at different positions have varying effects on the MPW due to their mitigation mechanisms, especially the cross-section area and the number of holes.

The cross-section area of the hood is limited by local terrain and construction cost, and a hood with a small cross-section $A_h = 155 \text{ m}^2$ is acceptable in engineering. However, the alleviation effects of the hood can be optimized by adjusting the number of holes at a reasonable cost. The pressure gradient at RH point when the same hood with various numbers of holes is installed at both the entrance and exit of the tunnel is shown in Figure 17a. The pressure gradient in the exit hood decreases compared to that in the tunnel influenced by the reflected expansion wave, which is more obvious as the number of holes increases. Due to the relief effect of the opening holes, the amplitude of the MPW emitted from the hood is alleviated further, as shown in Figure 17b. In contrast to that in Figure 11, the amplitude of the MPW decreases at first, and then increases as the number of holes increases. The amplitude of the MPW decreases to its lowest when $n = 16$, with $(\Delta p_m)_{\max} = 17.12 \text{ Pa}$, which drops by 86.85% compared to that without a hood.

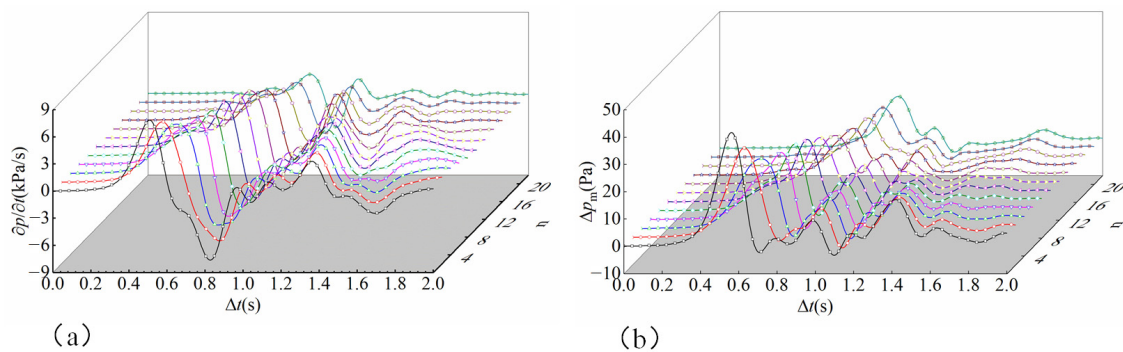


Figure 17. The effects of number of holes on tunnel aerodynamics: (a) Pressure gradient at RH point; (b) MPW at RM point.

In fact, the optimized hood can satisfy the alleviation requirements of the MPW at higher speeds. The maximum values of pressure gradient at RP point and the MPW at RM point are listed in Table 3. It can be seen that the pressure gradient in the tunnel and the MPW outside the hood increases rapidly with the train’s speed. The amplitude of the MPW can be reduced to 42.33 Pa by the optimized hood when the train passes through the tunnel at a speed of 500 km/h, which still satisfies the specification.

Table 3. Maximum values of the pressure gradient and MPW at different speeds.

Speed of Train	$(\partial p/\partial t)_{\max}$ (kPa/s)	$(\Delta p_m)_{\max}$ (Pa)
$v_t = 400$ km/h	8.97	17.12
$v_t = 450$ km/h	12.89	25.63
$v_t = 500$ km/h	18.00	42.33

5. Conclusions

In this paper, the aerodynamic effects of the oblique enlarged hood with opening holes installed at entrances or exits of tunnels are studied by a numerical method, and the effects of the hood geometry on the compression wave and the MPW are obtained. Then, the hood installed at both side of the tunnel is optimized. The main conclusions are as follows:

- (1) An oblique enlarged hood with opening holes at the tunnel entrance can reduce the MPW emitted from the tunnel by extending the rising process of the compression wave, which is divided into three stages corresponding to multiple peaks. The pressure gradient of the compression wave can be alleviated by properly increasing the oblique rate of the hood entrance and the cross-section area of the hood.
- (2) When the same type of hood is located at the exit of the tunnel, the MPW can be mitigated due to the relief effects of the opening holes and a larger spatial angle caused by the oblique exit. The amplitude of the MPW decreases with the increasing oblique rate of the hood exit and the number of opening holes in a certain range.
- (3) The MPW emitting from the tunnel can be greatly alleviated by the installation of the oblique enlarged hood with opening holes at both sides of the tunnel. Based on numerical simulation analysis, the tunnel hoods configuration that can satisfy the MPW mitigation requirement is obtained at the speed of 400 km/h. The optimized hood with $l_h = 80$ m, $A_t = 155$ m², $k = 1.25$, and $n = 16$ can reduce the MPW to satisfy the specification even at a speed of 500 km/h. The result can provide reference for the design of tunnel hoods at higher speeds.
- (4) However, the impact of oblique enlarged hood with opening holes located at the entrance and exit on aerodynamic effects such as transient pressure and passenger comfort will be further studied in the future.

Author Contributions: Conceptualization, W.M. and M.S.; methodology, M.S.; software, T.L.; validation, Y.F. and T.L.; investigation, Y.F.; data curation, Y.F. and T.L.; writing—original draft preparation, M.S.; writing—review and editing, W.M.; visualization, Y.F. and T.L. All authors have read and agreed to the published version of the manuscript.

Funding: This research was funded by the Open Foundation of State Key Laboratory for Track System of High-Speed Railway (Grant No. 2021YJ056).

Institutional Review Board Statement: Not applicable.

Informed Consent Statement: Not applicable.

Data Availability Statement: All data generated or analyzed during this study are included in this article and are available upon request by contact with the corresponding author.

Conflicts of Interest: Authors Weibin Ma and Yufei Fang were employed by the company China Academy of Railway Sciences Co., Ltd. The remaining authors declare that the research was conducted in the absence of any commercial or financial relationships that could be construed as a potential conflict of interest.

References

1. Uystepuyst, D.; William-Louis, M.; Monnoyer, F. 3D numerical design of tunnel hood. *Tunn. Undergr. Space Technol.* **2013**, *38*, 517–525. [[CrossRef](#)]
2. Kikuchi, K.; Iida, M. Optimization of Train Nose Shape for Reducing Micro-Pressure Wave Radiated from Tunnel Exit. *J. Low Freq. Noise Vib. Act. Control* **2011**, *30*, 1–19. [[CrossRef](#)]
3. Ozawa, S.; Maeda, T. Tunnel Entrance Hoods for Reduction of Micro-pressure Wave. *Q. Rep. RTRI* **1988**, *29*, 134–139.

4. Ozawa, S.; Maeda, T.; Matsumura, T.; Uchida, K. Micro-pressure waves radiating from exits of Shinkansen tunnels. *Q. Rep. RTRI* **1993**, *34*, 134–140.
5. Bellenoue, M.; Auvity, B.; Kageyama, T. Blind hood effects on the compression wave generated by a train entering a tunnel. *Exp. Therm. Fluid Sci.* **2002**, *25*, 397–407. [[CrossRef](#)]
6. Saito, S. Optimizing cross-sectional area of tunnel entrance hood for high speed rail. *J. Wind Eng. Ind. Aerodyn.* **2019**, *184*, 296–304. [[CrossRef](#)]
7. Fukuda, T.; Nakamura, S.; Saito, S. Effective Specifications for the Cross-sectional Area of Tunnel Hoods for Reducing Micro-pressure Waves. *Q. Rep. RTRI* **2022**, *63*, 31–36. [[CrossRef](#)]
8. Zhang, L.; Yang, M.Z.; Liang, X.F.; Zhang, J. Oblique tunnel portal effects on train and tunnel aerodynamics based on moving model tests. *J. Wind Eng. Ind. Aerodyn.* **2017**, *167*, 128–139. [[CrossRef](#)]
9. Zhang, L.; Yang, M.Z.; Niu, J.Q.; Liang, X.F.; Zhang, J. Moving model tests on transient pressure and micro-pressure wave distribution induced by train passing through tunnel. *J. Wind Eng. Ind. Aerodyn.* **2019**, *191*, 1–21. [[CrossRef](#)]
10. Zhang, L.; Liu, H.; Stoll, N.; Thurow, K. Influence of tunnel aerodynamic effects by slope of equal-transect ring oblique tunnel portal. *J. Wind Eng. Ind. Aerodyn.* **2017**, *169*, 106–116. [[CrossRef](#)]
11. Auvity, B.; Bellenoue, M. Effects of an opening on pressure wave propagation in a tube. *J. Fluid Mech.* **2005**, *538*, 269–289. [[CrossRef](#)]
12. Anthoine, J. Alleviation of Pressure Rise from a High-Speed Train Entering a Tunnel. *AIAA J.* **2009**, *47*, 2132–2142. [[CrossRef](#)]
13. Kim, D.H.; Cheol, S.Y.; Iyer, R.S.; Kim, H.D. A newly designed entrance hood to reduce the micro pressure wave emitted from the exit of high-speed railway tunnel. *Tunn. Undergr. Space Technol.* **2020**, *108*, 103728. [[CrossRef](#)]
14. Kim, D.H.; Seo, Y.C.; Kim, T.H.; Kim, H.D. Effects of detailed shape of air-shaft entrance hood on tunnel pressure waves. *J. Mech. Sci. Technol.* **2021**, *35*, 615–624. [[CrossRef](#)]
15. Howe, M.S. On the compression wave generated when a high-speed train enters a tunnel with a flared portal. *J. Fluids Struct.* **1999**, *13*, 481–498. [[CrossRef](#)]
16. Howe, M.S.; Iida, M.; Fukuda, T.; Maeda, T. Theoretical and experimental investigation of the compression wave generated by a train entering a tunnel with a flared portal. *J. Fluid Mech.* **2000**, *425*, 111–132. [[CrossRef](#)]
17. Howe, M.S. Design of a tunnel-entrance hood with multiple windows and variable cross-section. *J. Fluids Struct.* **2003**, *17*, 1111–1121. [[CrossRef](#)]
18. Howe, M.S.; Winslow, A.; Iida, M.; Fukuda, T. Rapid calculation of the compression wave generated by a train entering a tunnel with a vented hood. *J. Sound Vibr.* **2006**, *297*, 267–292. [[CrossRef](#)]
19. Murray, P.R.; Howe, M.S. Influence of hood geometry on the compression wave generated by a high-speed train. *J. Sound Vibr.* **2010**, *329*, 2915–2927. [[CrossRef](#)]
20. Zhang, J.; Wang, Y.G.; Han, S.; Wang, F.; Gao, G.L. A novel arch lattice-shell of enlarged cross-section hoods for micro-pressure wave mitigation at exit of maglev tunnels. *Tunn. Undergr. Space Technol.* **2023**, *132*, 104859. [[CrossRef](#)]
21. Mok, J.K.; Yoo, J. Numerical study on high speed train and tunnel hood interaction. *J. Wind Eng. Ind. Aerodyn.* **2001**, *89*, 17–29. [[CrossRef](#)]
22. Vardy, A.E.; Brown, J.M.B. Influence of Ballast on Wave Steepening in Tunnels. *J. Sound Vibr.* **2000**, *238*, 595–615. [[CrossRef](#)]
23. Adami, S.; Kaltenbach, H. Sensitivity of the wave-steepening in railway tunnels with respect to the friction model. In Proceedings of the 6th International Colloquium on: Bluff Body Aerodynamics and Applications, Milano, Italy, 20–24 July 2008.
24. Miyachi, T.; Saito, S.; Fukuda, T.; Sakuma, Y.; Ozawa, S.; Arai, T.; Sakaue, S.; Nakamura, S. Propagation characteristics of tunnel compression waves with multiple peaks in the waveform of the pressure gradient: Part 1: Field measurements and mathematical model. *Proc. Inst. Mech. Eng. Part F-J. Rail Rapid Transit* **2016**, *230*, 1297–1308. [[CrossRef](#)]
25. Fukuda, T.; Nakamura, S.; Miyachi, T.; Saito, S.; Kimura, N.; Matsunuma, M. Influence of ballast quantity on compression wavefront steepening in railway tunnels. *Proc. Inst. Mech. Eng. Part F-J. Rail Rapid Transit* **2020**, *234*, 607–615. [[CrossRef](#)]
26. Wang, H.L.; Lei, B.; Bi, H.Q.; Yu, T. Wavefront evolution of compression waves propagating in high speed railway tunnels. *J. Sound Vibr.* **2018**, *431*, 105–121. [[CrossRef](#)]
27. Rivero, J.M.; Gonzalez-Martinez, E.; Rodriguez-Fernandez, M. A methodology for the prediction of the sonic boom in tunnels of high-speed trains. *J. Sound Vibr.* **2019**, *446*, 37–56. [[CrossRef](#)]
28. Miyachi, T.; Fukuda, T. Experimental investigation of the effects of topography around the tunnel portal on micro-pressure waves. *Q. Rep. RTRI* **2014**, *55*, 235–240. [[CrossRef](#)]
29. Liu, F.; Niu, J.Q.; Zhang, J.; Li, G.X. Full-Scale Measurement of Micro-Pressure Waves in High-Speed Railway Tunnels. *J. Fluids Eng.-Trans. ASME* **2018**, *141*, 034501. [[CrossRef](#)]
30. Saito, S.; Miyachi, T.; Iida, M. Countermeasure for reducing micro-pressure wave emitted from railway tunnel by installing hood at the exit of tunnel. *Q. Rep. RTRI* **2013**, *54*, 231–236. [[CrossRef](#)]
31. Vardy, A.E. Generation and alleviation of sonic booms from rail tunnels. *Proc. Inst. Civ. Eng.-Eng. Comput. Mech.* **2008**, *161*, 107–119. [[CrossRef](#)]
32. Niu, J.Q.; Sun, Y.; Yu, Q.J.; Cao, X.L.; Yuan, Y.P. Aerodynamics of railway train/tunnel system: A review of recent research. *Energy Built Environ.* **2020**, *1*, 351–375. [[CrossRef](#)]
33. Versteeg, H.K.; Malalasekera, W. *An Introduction to Computational Fluid Dynamics: The Finite Volume Method*, 2nd ed.; Pearson/Prentice Hall: Harlow, UK, 2007.

34. Ku, Y.C.; Rho, J.H.; Yun, S.H.; Kwak, M.H.; Kim, K.H.; Kwon, H.B.; Lee, D.H. Optimal cross-sectional area distribution of a high-speed train nose to minimize the tunnel micro-pressure wave. *Struct. Multidiscip. Optim.* **2010**, *42*, 965–976. [[CrossRef](#)]
35. Liu, F.; Yao, S.; Liu, T.; Zhang, J. Analysis on aerodynamic pressure of tunnel wall of high-speed railways by full-scale train test. *J. Zhejiang Univ. (Eng. Sci.)* **2016**, *50*, 2018–2024.

Disclaimer/Publisher’s Note: The statements, opinions and data contained in all publications are solely those of the individual author(s) and contributor(s) and not of MDPI and/or the editor(s). MDPI and/or the editor(s) disclaim responsibility for any injury to people or property resulting from any ideas, methods, instructions or products referred to in the content.